

8-22-2011

# Glucose Biosensor Using Electrospun Mn<sub>2</sub>O<sub>3</sub>-Ag Nanofibers

Shan Huang  
shanhangel@hotmail.com

---

## Recommended Citation

Huang, Shan, "Glucose Biosensor Using Electrospun Mn<sub>2</sub>O<sub>3</sub>-Ag Nanofibers" (2011). *Master's Theses*. 147.  
[http://digitalcommons.uconn.edu/gs\\_theses/147](http://digitalcommons.uconn.edu/gs_theses/147)

This work is brought to you for free and open access by the University of Connecticut Graduate School at DigitalCommons@UConn. It has been accepted for inclusion in Master's Theses by an authorized administrator of DigitalCommons@UConn. For more information, please contact [digitalcommons@uconn.edu](mailto:digitalcommons@uconn.edu).

*Glucose Biosensor Using Electrospun Mn<sub>2</sub>O<sub>3</sub>-Ag Nanofibers*

Shan Huang

B.S., Hunan Normal University, 2009

A Thesis Submitted in  
Partial Fulfillment of the  
Requirements for the Degree of  
Masters of Science at the  
University of Connecticut

2011

***APPROVAL PAGE***

Master of Science Thesis

**Glucose Biosensor Using Electrospun Mn<sub>2</sub>O<sub>3</sub>-Ag Nanofibers**

Presented by Shan Huang, B.Sc.

Major Advisor \_\_\_\_\_

Yu Lei

Associate Advisor \_\_\_\_\_

Baikun Li

Associate Advisor \_\_\_\_\_

William Mustain

University of Connecticut

2011

## *Acknowledgements*

I am heartily thankful to my advisor Dr. Lei, who gives me the guidance and the opportunity to participate in the program, and advises me in the theory field.

I would like to show my gratitude to my associate advisors Dr. Li and Dr. Mustain for their instructive suggestions and valuable advices.

It is also a pleasure to thank my lab mates, who give me a lot of help and suggestion in my research.

I am grateful for the support and encouragement from my friends. I could not have finished this without my friends' help, understanding, and moral support.

Most of all, I would like to express my never ending love to my parents, for their unconditional supports and care.

## ***Table of Contents***

Glucose Biosensor Using Electrospun Mn <sub>2</sub> O <sub>3</sub> -Ag Nanofibers.....	i
APPROVAL PAGE.....	ii
Acknowledgements.....	iii
Table of Contents.....	iv
Chapter 1 Introduction.....	1
<b><i>1.1 Diabetes and Glucose Detection</i></b> .....	1
<b><i>1.2 Enzyme-based Glucose Biosensor in Batch</i></b> .....	2
1.2.1 Glucose Oxidase-based glucose Biosensor.....	2
1.2.2 Glucose Dehydrogenase-based Glucose Biosensor .....	3
<b><i>1.3 Nonenzymatic Glucose Sensor in Batch</i></b> .....	4
1.4 Continuous Glucose Detection .....	7
<b><i>1.5 Electrospinning Nanofibers</i></b> .....	9
<b><i>1.6 Objective</i></b> .....	11
Chapter 2 Direct Electrochemistry and Electrocatalysis of Glucose Oxidase on Electrospun Mn <sub>2</sub> O <sub>3</sub> -Ag Nanofibers -Towards Glucose Biosensing.....	13
Abstract.....	13
2.1 Experiment .....	14
2.1.1 Reagents.....	14

2.1.2	Preparation of Mn <sub>2</sub> O <sub>3</sub> -Ag nanofibers.....	14
2.1.3	Preparation of Mn <sub>2</sub> O <sub>3</sub> -Ag nanofibers modified glassy carbon electrode...	15
2.1.4	Apparatus and electrochemical measurement.....	16
2.2	Results and discussion.....	17
2.2.1	Characterization of Mn <sub>2</sub> O <sub>3</sub> -Ag nanofibers.....	17
2.2.2	Electrochemical characterization of Mn <sub>2</sub> O <sub>3</sub> -Ag nanofibers-GOD modified electrode.....	20
2.2.3	Electrochemical reduction of O <sub>2</sub> at the modified electrodes and amperometric glucose biosensing.....	25
2.3	Conclusion.....	30
Chapter 3	Conclusions, Future Prospects and Challenges.....	31
Reference	.....	33

# *Chapter 1*

## *Introduction*

### *1.1 Diabetes and Glucose Detection*

Diabetes mellitus is a worldwide public health problem. This metabolic disorder results from insulin deficiency and hyperglycemia and is reflected by blood glucose concentrations higher than the normal range of 80-120 mg/ dL (4.4-6.6 mM) [1]. As it reported by International Diabetes Federation, at the year of 2000, at least 171 million people worldwide suffer from diabetes, and the population is estimated to reach 366 million by the year of 2030 [2]. The crude estimated prevalence of diabetes in adults in the United States (US) has been reported to be 9.6% (20.4 million) in 2003-2006 [3]. This disease is one of the leading causes of death and disability in the world. The complications of diabetes are numerous, including high risks of heart disease, kidney failure, or blindness. Such complications can be greatly reduced through stringent personal control of blood glucose using glucose biosensor. Millions of diabetics test their blood glucose levels daily, making glucose the most commonly tested analyte. Glucose biosensors account for about 85% (around 5 billion US dollar) of the entire biosensor market [4]. According to a recent report by Global Industry Analysts, Inc., the global market for glucose biosensors and test strips will reach US \$11.5 billion by 2012. Therefore, due to its serious health complications and the extremely large financial burden caused by diabetes, the reliable detection of glucose is becoming incredibly important in managing diabetes and reducing its financial costs. Currently, the methods

for glucose detection can be classified into two different types: enzymatic and non-enzymatic. In addition, according to the detection mode, glucose detection can be divided into disposable detection (for single use) and continuous detection. In the following section, both enzyme-based and non-enzyme-based glucose detections operated in disposable mode are discussed in detail, and continuous glucose detection is briefly introduced.

## ***1.2 Enzyme-based Glucose Biosensor in Batch***

### ***1.2.1 Glucose Oxidase-based glucose Biosensor***

Due to its high selectivity to glucose, and high activity over a broad range of pH, ionic strength, and temperature, glucose oxidase (GOD)-based glucose detection allows less stringent conditions during the manufacturing process and storage, and thus has been widely applied in glucose detection [5-12]. GOD is a slightly elongated globular protein [13]. In order to be a functional biocatalyst, GOD requires a redox cofactor - flavin adenine dinucleotide (FAD). During glucose oxidation, FAD serves as the initial electron acceptor and is reduced to FADH<sub>2</sub>, which is regenerated by reacting with oxygen, leading to the formation of hydrogen peroxides ( $glucose + O_2 \xrightarrow{GOD} gluconolactone + H_2O_2$ ) [1, 14]. Thus two general strategies used for the GOD-based electrochemical sensing of glucose are: by measuring oxygen consumption [15-18] and by measuring the amount of hydrogen peroxide produced through the enzyme reaction (the first generation glucose biosensor) [19-30]. However, the performance of GOD-based glucose biosensors is usually limited by the electron transfer between the enzyme and the electrode because the

catalytic active centers of GOD are covered by the protein shell and thus the direct electron transfer from the enzyme to the electrode is quite difficult [31].

Varieties of materials have been employed to improve the electron transfer process between GOD and electrode [32], in which electrospun metal oxide nanofibers and noble metal nanofibers have attracted increasing attention [33-36]. Nanomaterials have unique advantages in immobilizing enzyme and retaining its bioactivity due to their high surface to volume ratio, the favorable microenvironment, and the enhanced direct electron transfer between the enzyme's active sites and the electrode [37]. Thus the glucose biosensor's performance can be potentially improved by using novel functional nanostructured materials.

### ***1.2.2 Glucose Dehydrogenase-based Glucose Biosensor***

Glucose dehydrogenase (GDH) is another choice for enzyme-based amperometric biosensing of glucose. The GDH family includes GDH-pyrroquinolinequinone (PQQ) [38-40] and GDH-nicotinamide-adenine dinucleotide (NAD) [41]. However, the construction of glucose biosensors based on GDH requires a source of NAD<sup>+</sup> and a redox mediator to lower the overvoltage for oxidation of the NADH product:



Quinoprotein GDH can be used in connection to a pyrroloquinoline quinone (PQQ) cofactor during the reaction:



While eliminating the need for a NAD<sup>+</sup> cofactor, such PQQ enzymes have not been widely used owing to their limited stability.

However, GDH still suffer from big issue in distinguishing glucose from other sugars such as maltose. As it warned by U.S. FDA, other sugars present in serum can bring error in glucose concentration thus affects the insulin injection which is fatal to the patients. (<http://www.fda.gov/MedicalDevices/Safety/AlertsandNotices/PublicHealthNotifications/ucm176992.htm>).

### ***1.3 Nonenzymatic Glucose Sensor in Batch***

Due to the insufficient stability, simplicity and reproducibility of the enzymatic glucose biosensor, which are hard to overcome, enzymeless glucose sensor has been studied and improved. Continuous efforts to realize this idea have been made since early studies on the electrochemistry of glucose itself [42-44]. In recent years, considerable attention has been given to enzyme-free electrodes with good glucose sensitivity and selectivity. Precious metals and metal alloys (e.g. Au [45], Pt [46], Ni [47], Cu [48], Pt-Pb [49], Ni-Cu [50], and Au-Ag [51]) have been extensively investigated towards nonenzymatic glucose sensors. Although both bulk and nanoscale materials are used for electro-catalyzing glucose oxidation, the nanostructured materials have been triggering considerable research activities due to their large surface-to-volume ratio which can greatly improve the sensitivity or selectivity and potentially minimize the adsorption of poisoning intermediates.

On a metal surface, interconversion can happen between two hemiacetal-types of glucose ( $\alpha$ -glucose and  $\beta$ -glucose) to each other through acid-catalyzed hydrolysis via aldehyde-type glucose ( $\gamma$ -glucose):



All these three types of glucose can be converted to glucono lactone through different pathway. For both  $\alpha$ -glucose and  $\beta$ -glucose, because the acidity of hemiacetalic OH group is stronger than alcoholic OH, the hydrogen atom tethered to C<sub>1</sub> carbon is activated. Thus the product of electrochemical oxidation of  $\alpha$ -glucose and  $\beta$ -glucose is glucono- $\delta$ -lactone. While the electrochemical oxidation of  $\gamma$ -glucose produces gluconic acid directly. Regardless of whether the glucono- $\delta$ -lactone is involved as an intermediate or not, gluconic acid is the final stable product of two-electron oxidation of glucose [52].

Enzymeless glucose sensor has overcome some essential drawbacks of the biosensor based on GOD or GOH. Nonenzymatic glucose biosensor can work in severe condition, For example, pure platinum with nanoporous surface shows high sensitivity and selectivity to glucose even after exposure to 1M NaOH or H<sub>2</sub>SO<sub>4</sub> [46]. For an enzyme modified electrode, the most important factor in fabrication is enzyme immobilization, and one or more enzyme layers should be placed on the bare electrode through carefully optimized process. There have been reported a number of methods for enzyme immobilization, such as direct adsorption, sol-gel entrapment, cross-linking, all of which are cost and time consuming. Regardless the immobilization techniques and the choice of enzyme, enzymatic glucose biosensor can not get rid of the intrinsic uncertainty of biological components bring from the modification process. In this respect, the non-enzymatic sensor is an attractive alternative.

However, the sensing utility of these electrode materials is very limited due to drawbacks such as low sensitivity, poor selectivity, and high costs, and also suffer from

the poisoning of chloride ions [46, 53, 54]. Therefore, there are considerable demands for development of a novel cost-effective, sensitive, selective, and reliable enzyme-free glucose sensor [55]. Recently, the PI's group and other groups have been exploring metal oxides such as nanoscale  $\text{Co}_3\text{O}_4$  [7], NiO [56], CuO [57, 58] and bulk metal oxides ( $\text{Cu}_2\text{O}$ ,  $\text{RuO}_2$ , CoO and NiO) [59] in the construction of a variety of enzyme-free glucose sensors. Besides, carbon nanotubes alone can be employed in glucose detection [53, 55] or used as a cofactor to improve the sensitivity of metal or metal oxide based non-enzymatic glucose sensors (e.g. gold nanoparticles/MWNTs nanocomposites [60],  $\text{Cu}_2\text{O}$ /MWNTs nanocomposites [61] and electrodeposited  $\text{MnO}_2$  on MWNTs [62]). Recent activity in practical non-enzymatic glucose sensor has been focusing on major advances in electrocatalysis. The first goal was to enhance the sensitivity towards glucose. Another goal was to reduce the interference of co-existing electroactive species. Most of the reported non-enzymatic glucose sensors lack a glucose recognition unit. Thus, it is difficult to distinguish glucose from other electroactive interferences (e.g. uric acid, ascorbic acid, acetaminophen, etc.) and other sugars (e.g. maltose). In addition, the majority of reported non-enzymatic glucose sensors require a strong alkaline environment to oxidize glucose, while in normal condition, the blood physiological pH is around pH 7.4. In order to use the sensing platform similar to current enzyme-based test strips, new creative ideas are needed to realize and implement the alkaline environment on the screen printed test strips.

## ***1.4 Continuous Glucose Detection***

To address these shortcomings of single use and to provide more frequent measurements, new glucose-sensing strategies have been proposed. The first strategy is continuous glucose monitoring systems. Continuous ex vivo and in vivo monitoring of blood glucose were first proposed in 1970's and 1980's, respectively.[63, 64] In vivo continuous glucose monitoring would generate real-time data about the change of blood glucose levels and have relatively constant operating temperature (body temperature). However, unfortunately, the development of reliable implantable glucose sensor is still very challenging as undesirable interactions between the implanted device and biological medium cause rapid deterioration of the sensor performance upon implantation.[1] In addition, due to surface fouling of the electrode by proteins and coagulation factors and the risk of thromboembolism, most of the continuous glucose detection does not measure blood glucose directly, and their stability and calibration of the reading to blood glucose levels have also proven difficult to overcome.[4] Despite extensive research efforts in these area, no reliable method is presently available for implantable continuous glucose monitoring and it is still uncertain if a reliable implantable glucose sensor will become available in the near future.[1] Therefore, extensive efforts have been devoted over the past decade toward the design of subcutaneously implantable needle-type electrodes measuring glucose concentrations in interstitial fluid, which reflect the blood glucose level.[65-67] Even though these 'under-the-skin' devices can display updated real-time glucose concentrations every one to five minutes, the accuracy of these innovative devices is inferior to traditional strip-based glucose biosensors[14] (thus requiring periodic strip calibrations), and their lifetime is very limited (to five to seven days) due to

similar biofouling problems.[68] Subcutaneous continuous glucose monitoring can also be achieved without direct contact between the interstitial fluid and transducer by using the microdialysis technique.[69, 70] For example, glucoDay (Menarini, Florence, Italy) and SCGM (Roche, Mannheim, Germany) are based on a microdialysis technique. However, major challenges to subcutaneous continuous glucose monitoring, including biocompatibility, calibration, drift and long-term stability, specificity, linearity, and miniaturization, hamper its routine clinical usefulness. The second strategy is non-invasive glucose monitoring system. Non-invasive glucose analysis is another goal of glucose sensor technology and significant efforts have been made to achieve this goal. Optical or transdermal approaches are the most common noninvasive glucose sensing methods [71, 72]. The optical glucose sensors use physical properties of light in the interstitial fluid or the anterior chamber of the eye, and different optical techniques such as polarimetry [73, 74], Raman spectroscopy [75], infrared absorption spectroscopy [76], photoacoustics [77], and optical coherence tomography [78] have been studied for non-invasive glucose detection. However, due to the complication of tissues, reliable non-invasive optical glucose measuring method is still unavailable. On the other hand, as a first transdermal glucose sensor approved by the U.S. FDA, the GlucoWatch Biographer (Cygnus, Inc., Redwood City, CA, USA), is a watch-like electrochemical device based on transdermal extraction of interstitial fluid by reverse iontophoresis. However, it has not gained wide acceptance due to long warm up time, false alarm, inaccuracy, skin irritation and sweating. Finally, the GlucoWatch Biographer was withdrawn from the market in 2008. The third strategy, which is been researched in recently several years, is to replace

currently used GOD or GDH-based test strips with non-enzymatic glucose test strips to allow highly reliable and frequent low-cost measurements.

### ***1.5 Electrospinning Nanofibers***

Electrospinning is a process of applying a high voltage electric field (several to tens of kilovolts) to generate electrically charged jets from polymer solutions or melts and further to produce polymer (nano) fibers. This technique is quite similar with the commercial process for drawing microscale fibers, however it is more suitable for generating nanofibers, because the elongation can be accomplished by a contactless scheme through the application of an external electric field [79]. There are four basic components required for an electrospinning process, including a high voltage supplier, a needle with small diameter, a syringe pump, and a collecting screen. Although the electrospinning process has been widely applied to generate fibers ranging from nanoscale to microscale, the mechanism of the fiber formation is quite complicated, which has not been fully understood. It is generally believed that the electrospinning process can be divided into four steps: (1) the sufficiently high voltage is applied to a liquid droplet; (2) the body of the liquid becomes charged, and electrostatic repulsion counteracts the surface tension and droplet is stretched, at a critical point a stream of liquid erupts from the surface. This point of eruption is known as the Taylor cone. (3) ejection of charged polymer jet; and (4) collection of the fibers on the collector with any geometry. The elongation and thinning of the fiber resulting from this bending instability leads to the formation of uniform fibers with nanometer-scale diameters. After ejected

from the tip, the jet moves towards the oppositely charged collector, and dry fibers were collected due to the solvent evaporation [80-82]. Based on the description above, one can see that the electrospinning process can be potentially affected by many factors such as solution properties (e.g. viscosity, elasticity, conductivity, and surface tension), operating conditions (polymer gel feed rate, electric potential at the tip, and the gap between the tip and the collector), and ambient parameters (e.g. temperature, humidity and air velocity) in the electrospinning chamber [80, 83].

Although the setup for electrospinning is quite straightforward, the inner mechanism is rather complicated specially the involving of complex electro-fluid-mechanical issues. It has been proved by recent experiment that in electrospinning, the thinning of a jet is mainly caused by the bending instability associated with the electrified jet [84]. According to their research, the jet was initially a straight line and then became unstable. And the coneshaped, instability region is composed of multiple jets. The surface to volume ratio of a nanofibers can be greatly increased when the surface of the nanofibers become porous. And the enhanced surface area is beneficial to numerous applications such as catalysis, filtration, absorption and tissue engineering. Generally, generation of porous surface on a bulk electrospinning nanofiber can be realized through two different ways. The first one is based on the selective removal of a component from nanofibers made of a composite or blend material, while the other one involved the use of phase separation of different polymers during electrospinning under the application of proper spinning parameters [84]. Both the pore size and the density are controllable by changing the parameters. For instance, in PLA/PVP electrospinning nanofibers, more porosity can be generated when the two material are loaded in equal amounts comparing to the

corresponding product by different proportion of PLA/PVP. It can be attributed to the rapid phase separation and solidification in the spinning jet [85]. The formation of pores is also affected by the solvent vapor pressure and the humidity in atmosphere. The cooling effect which comes from rapid evaporation of a highly volatile solvent might induce the polymers to separate into different phases in liquid jet. Because of evaporative cooling and condensation, water droplets could also be formed within the fibers to promote the formation of porous nanofibers [86].

The electrospun nanofibers exhibit several unique features which enable the prevalent utilization of them. Because electrospinning is a continuous process without any contact force for elongation, the fibers can be as long as several kilometers, and can be further assembled into a 3D mat with porous structure. At the same time, electrospun fibers can have a thinner diameter and surface to volume ratio, due to the presence of porous structure. Also, due to the simple fabrication process and the diversity of suitable materials, the electrospinning technique and its resultant nanofiber product have attracted increasing attention. These properties potentiate the use of the electrospun nanofibers in various applications such as reinforced composites, nanofiber-based membranes, nanofiber-based support for enzyme and catalyst [79].

## **1.6 Objective**

Although the glucose detection methods based on GOD suffer from many drawbacks, glucose oxidase-based glucose detection method is still widely used in current blood glucose management due to its good selectivity and high affinity with glucose. Up to date,

a variety of glucose sensors based on different materials have been reported for the detection of glucose, while electrochemical glucose biosensors with low detection limit, high sensitivity, excellent selectivity, reproducibility and stability, as well as low cost, are always highly demanded for quantitative determination of glucose. The major goal of this research focused on developing a GOD-based glucose biosensor using electrospun metal oxide-noble metal nanofibers. Specifically, we were seeking to employ electrospun manganese oxide-silver ( $\text{Mn}_2\text{O}_3\text{-Ag}$ ) nanofibers as the novel functional nanomaterial for GOD immobilization in order to accelerate the electron transfer between GOD and the electrode. The high surface-to-volume ratio and high porosity of  $\text{Mn}_2\text{O}_3\text{-Ag}$  nanofibers could offer large surface for enzyme immobilization, thus achieving high loading of GOD. On the other hand, electron transfer and electrocatalytic property are expected to be greatly enhanced because of the excellent electrical and catalytic properties of  $\text{Mn}_2\text{O}_3$  and Ag. The electrochemistry of GOD on  $\text{Mn}_2\text{O}_3\text{-Ag}$  nanofibers and the performance of the developed  $\text{Mn}_2\text{O}_3\text{-Ag-GOD}$  glucose biosensor based on oxygen reduction are systematically investigated and reported in Chapter 2.

## *Chapter 2*

### *Direct Electrochemistry and Electrocatalysis of Glucose Oxidase on Electrospun Mn<sub>2</sub>O<sub>3</sub>-Ag Nanofibers -Towards Glucose Biosensing*

#### *Abstract*

The highly porous Mn<sub>2</sub>O<sub>3</sub>-Ag nanofibers were fabricated by a facile two-step procedure (electrospinning and calcination) and then employed as the immobilization matrix for glucose oxidase (GOD) to construct an amperometric glucose biosensor. A notable enhancement of direct electron transfer between GOD and the electrode is observed at the Mn<sub>2</sub>O<sub>3</sub>-Ag-GOD modified electrode with a fast electron transfer rate constant. The biosensor also shows fast response to glucose, high sensitivity (40.60  $\mu\text{A}\cdot\text{mM}^{-1}\cdot\text{cm}^{-2}$ ), low detection limit (1.73  $\mu\text{M}$  at S/N=3), low  $K_{m,app}$  value and excellent selectivity. These results indicate that the novel Mn<sub>2</sub>O<sub>3</sub>-Ag nanofibers-GOD composite has great potential application in oxygen-reduction-based glucose biosensing.

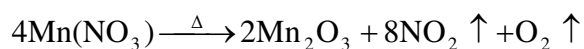
## ***2.1 Experiment***

### ***2.1.1 Reagents***

GOD (129,900 units/g), manganese (II) nitrate tetrahydrate, Nafion perfluorinated resin solution (20 wt% in lower aliphatic alcohols/H<sub>2</sub>O) and poly(vinylpyrrolidone) (PVP, MW = 1,300,000) were purchased from Sigma-Aldrich. Silver nitrate, ascorbic acid (AA), uric acid (UA) and D-(+)-glucose were supplied by Acros Organics. 0.1 M phosphate buffer solutions with various pH values were prepared by mixing stock standard solutions of Na<sub>2</sub>HPO<sub>4</sub> and NaH<sub>2</sub>PO<sub>4</sub> and adjusting the pH values with NaOH and H<sub>3</sub>PO<sub>4</sub> solution. All solutions used in the experiments were prepared with deionized water (18.2 MΩ-cm) generated by a Barnstead water system.

### ***2.1.2 Preparation of Mn<sub>2</sub>O<sub>3</sub>-Ag nanofibers***

44 wt% Mn(NO<sub>3</sub>)<sub>2</sub>, 11 wt% AgNO<sub>3</sub> and 44 wt% PVP was dissolved in DMF. The solution was kept under magnetic stirring for 2h and then loaded into a plastic syringe equipped with a 23-gauge needle made of stainless steel. Electrospinning process was conducted at an applied voltage of 20 kV with a feeding rate of 0.3 mL/h and a collection distance of 15 cm. The nanofibers were collected on aluminum foil and then calcined under air atmosphere at 500 °C for 3 h for the degradation of PVP and the decomposition of Mn(NO<sub>3</sub>)<sub>2</sub> and AgNO<sub>3</sub>:



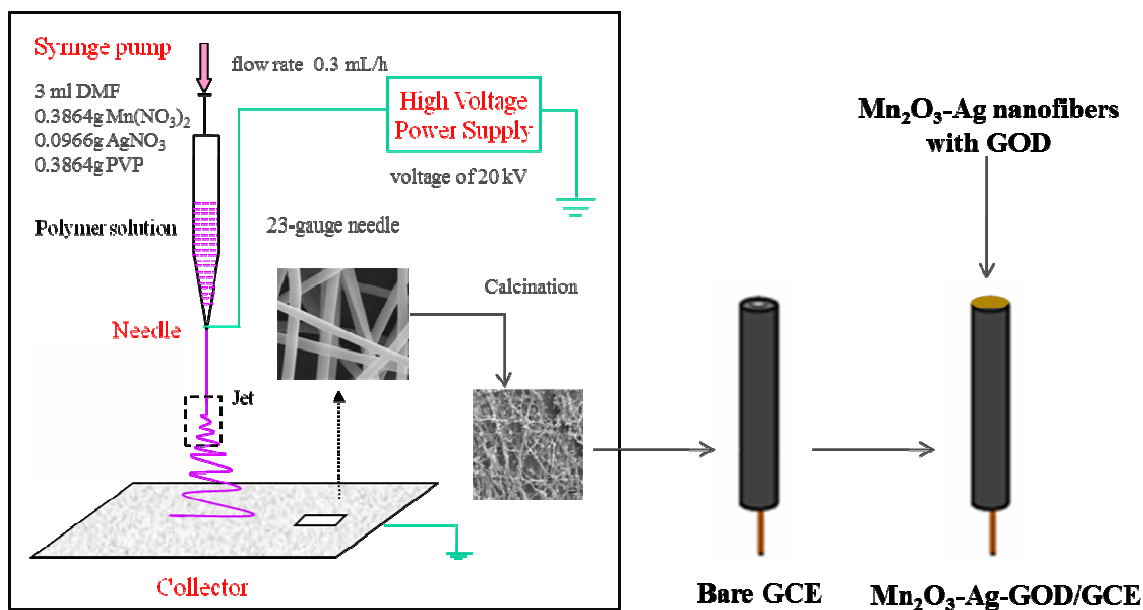


Figure 1. Schematic illustration of the two-step fabrication of  $\text{Mn}_2\text{O}_3\text{-Ag}$  nanofibers and modification of  $\text{Mn}_2\text{O}_3\text{-Ag-GOD}$  electrode.

### 2.1.3 Preparation of $\text{Mn}_2\text{O}_3\text{-Ag}$ nanofibers modified glassy carbon electrode

Glassy carbon electrode (GCE, dia. 3 mm) was polished with 1  $\mu\text{m}$  and 0.05  $\mu\text{m}$  alumina slurries sequentially, and then rinsed with DI water. After that, the electrode was sonicated in deionized water, and finally dried under ambient conditions. To prepare the modified GCE, 10 mg  $\text{Mn}_2\text{O}_3\text{-Ag}$  nanofibers were dispersed in 1 mL of 1 wt% diluted Nafion solution (in 0.1 M pH 7 phosphate buffer) under sonication for 30 min. GOD (100 mg/mL in 0.1 M pH 7 phosphate buffer) was then added into the  $\text{Mn}_2\text{O}_3\text{-Ag-Nafion}$  dispersion at a 1:1 (v/v) ratio, thus the mixture consists of 5 mg/ml  $\text{Mn}_2\text{O}_3\text{-Ag}$  nanofibers,

0.5 wt% Nafion and 50 mg/mL GOD. After another 10 min sonication, 5  $\mu$ L of  $\text{Mn}_2\text{O}_3$ -Ag-Nafion-GOD mixture was dropped on the GCE (denoted as  $\text{Mn}_2\text{O}_3$ -Ag-GOD/GCE), and then dried for 30 min in the air. To prevent the leakage of GOD in subsequent experiments and maintain the good performance of the modified electrode, the as-prepared electrode was exposed to glutaraldehyde vapor for GOD cross-linking.  $\text{Mn}_2\text{O}_3$ -Nafion-GOD modified GCE ( $\text{Mn}_2\text{O}_3$ -GOD/GCE) and Nafion-GOD modified GCE (GOD/GCE) were also prepared as the control electrodes.

#### ***2.1.4 Apparatus and electrochemical measurement***

A JEOL 6335F field-emission scanning electron microscope (SEM) was used to examine the morphology and the size of the as-prepared nanofibers. More detailed morphology and selected area electron diffraction (SAED) patterns of  $\text{Mn}_2\text{O}_3$ -Ag nanofibers were obtained with a Tecnai T12 transmission electron microscope (TEM) operated at 120 kV. XRD pattern was obtained with an Oxford diffraction Xcalibur<sup>TM</sup> PX Ultra with ONYX detector to study the crystal structure of  $\text{Mn}_2\text{O}_3$ -Ag nanofibers. Cyclic voltammetry (CV) measurements were performed on a Model CHI 601 C Electrochemical Workstation (CH Instruments, USA). All experiment were conducted using a three-electrode electrochemical cell (10-mL volume with a working volume of 5 mL), with a working electrode, an Ag/AgCl reference electrode, and a platinum wire counter electrode. For amperometric detection, all measurements were performed by applying an appropriate potential to the working electrode and allowing the transient background current to decay to a steady-state value, before the addition of the analyte. A stirred solution was employed to provide convective transport. For the study of direct

electron transfer of GOD, the solution was purged with high purity nitrogen gas (99.99%, Airgas) for 15 min and a nitrogen atmosphere was maintained over the solution.

## 2.2 Results and discussion

### 2.2.1 Characterization of $Mn_2O_3$ -Ag nanofibers

SEM was first employed to investigate the morphology of the  $Mn_2O_3$ -Ag nanofibers. Figure 2A presents a typical SEM image of electrospun precusory PVP- $Mn(NO_3)_2$ - $AgNO_3$  nanofibers. After calcination, the as-prepared  $Mn_2O_3$ -Ag composite nanofibers (Figure 2B) exhibit a porous network structure and their surfaces are no longer as smooth

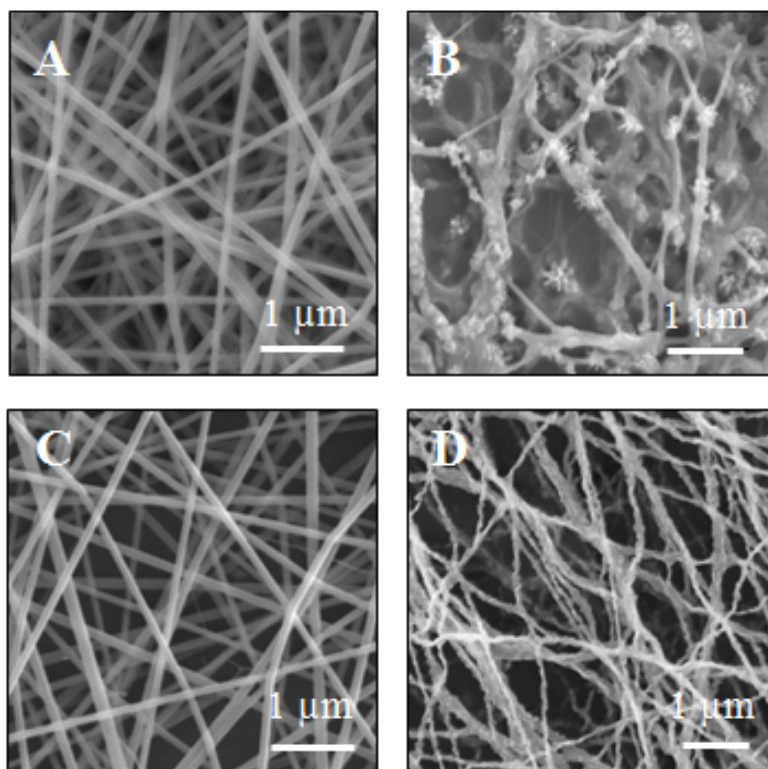


Figure 2. SEM images of (A) PVP- $Mn(NO_3)_2$ - $AgNO_3$  nanofibers, (B)  $Mn_2O_3$ -Ag nanofibers, (C) PVP- $Mn(NO_3)_2$  nanofibers, and (D)  $Mn_2O_3$  nanofibers, respectively.

as the precursory nanofibers. Such feature endows the nanofibers with high surface-to-volume ratio which could provide not only a large surface area for GOD loading but also a large interface for direct electron transfer of GOD. As a comparison, the nanofibers prepared by single metal salt ( $\text{Mn}(\text{NO}_3)_2$ ) with PVP and its calcined product ( $\text{Mn}_2\text{O}_3$  nanofibers) are presented in Figure 2C and D, respectively. One can see that the precursory nanofibers electrospun from PVP containing two mixed metal salts ( $\text{Mn}(\text{NO}_3)_2$  and  $\text{AgNO}_3$ ) had a smaller average diameter (ca. 20 nm smaller) which might be resulted from the increase of solution conductivity, while the morphology of its corresponding calcined  $\text{Mn}_2\text{O}_3$ -Ag nanofibers is slightly different from that of  $\text{Mn}_2\text{O}_3$  nanofibers and display many nanoscale protrusions which can also be clearly observed in the TEM image (Figure 2A).

Figure 3A shows a typical TEM image for single  $\text{Mn}_2\text{O}_3$ -Ag nanofiber. One can see that the  $\text{Mn}_2\text{O}_3$ -Ag nanofibers obtained after calcination are composed of numerous nanoparticles which coalesce together, thus generating highly porous nanofibers. Such porous nanofibers could provide more catalytic sites on the surface of  $\text{Mn}_2\text{O}_3$ -Ag nanofibers and thus greatly favor the subsequent electrochemical detection of glucose. The element mapping of Ag, Mn, and O (insets of Figure 3A) indicates the homogenous distribution of Ag and  $\text{Mn}_2\text{O}_3$ . Figure 3B displays the corresponding selected area diffraction pattern, indicating the polycrystalline structure of the nanofibers. The chemical composition of the nanofibers was further examined using X-ray energy dispersive spectroscopy (EDX). As shown in Figure 3C, the presence of Ag, Mn and O peaks indicates the constitution of the composite nanofibers (C and Cu peaks come from the TEM grid). The composition and crystal structure were also characterized by XRD

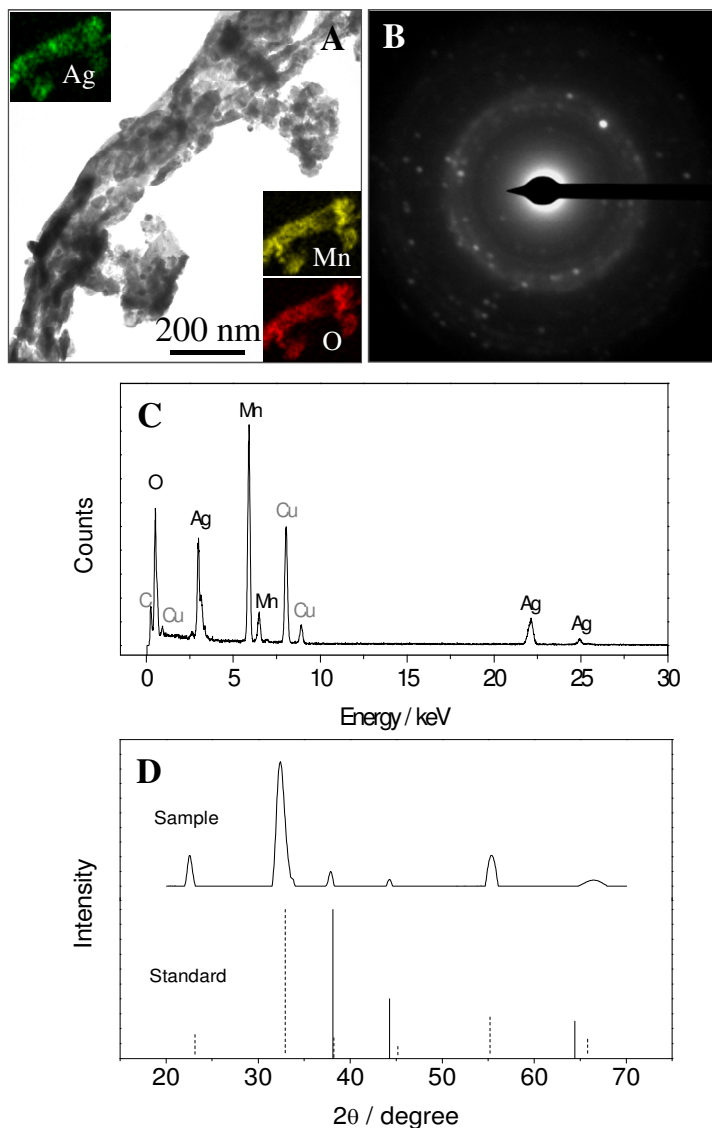


Figure 3. (A) A typical TEM image of one Mn<sub>2</sub>O<sub>3</sub>-Ag nanofiber; insets show the EDX mapping of Ag, Mn and O elements. (B) SAED pattern of Mn<sub>2</sub>O<sub>3</sub>-Ag nanofibers. (C) EDX spectrum of Mn<sub>2</sub>O<sub>3</sub>-Ag nanofibers (carbon and copper peaks come from the copper-carbon grid of TEM). (D) XRD patterns for the standard values of JCPDS 41-1442 (Mn<sub>2</sub>O<sub>3</sub>, dash line), JCPDS 04-0783 (Ag, solid line) and the as-prepared porous Mn<sub>2</sub>O<sub>3</sub>-Ag nanofibers, respectively.

(Figure 3D). The XRD spectrum of Mn<sub>2</sub>O<sub>3</sub>-Ag nanofibers matches the combination of the standard spectrum of JCPDS 41-1442 (Mn<sub>2</sub>O<sub>3</sub>) and JCPDS 04-0783 (Ag). The formation of face-centered cubic crystalline Mn<sub>2</sub>O<sub>3</sub> is revealed by the diffraction peaks at

$2\theta$  values of 32.951, 38.234, 45.178, 49.347, 55.189, 65.806, corresponding to (111), (200), (220), (311), (222), and (400) crystal planes, respectively; while the diffraction peaks at  $2\theta$  values of 38.116, 44.277, and 64.426, which correspond to (111), (200), and (220) crystal planes respectively, indicates the formation of cubic crystalline Ag.

### 2.2.2 Electrochemical characterization of $Mn_2O_3$ -Ag nanofibers-GOD modified electrode

The electrochemical behavior of the immobilized GOD on the  $Mn_2O_3$ -Ag nanofibers were first investigated using cyclic voltammetry in  $N_2$  de-aerated 0.1 M pH 7 phosphate buffer at the scan rate of 100 mV/s. Figure 4 presents the CVs of GCEs modified with three different composite films. No obvious redox peaks can be observed in the CV of a

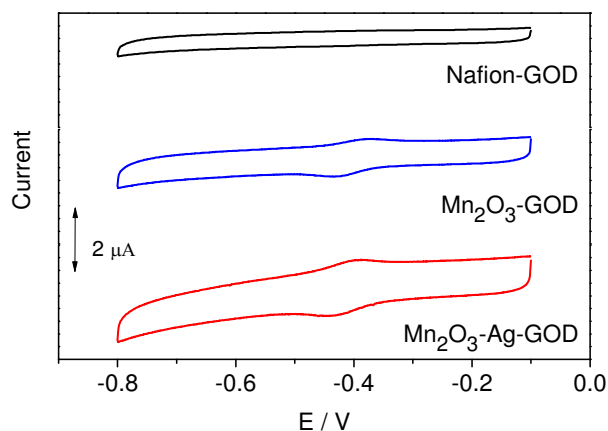


Figure 4. Cyclic voltammograms of the GOD/GCE,  $Mn_2O_3$ -GOD/GCE,  $Mn_2O_3$ -Ag-GOD/GCE in  $N_2$  de-aerated 0.1 M pH 7 phosphate buffer at a scan rate of 100 mV/s.

Nafion-GOD modified glassy carbon electrode (GOD/GCE, control electrode) because the catalytic active centers of GOD are covered by the electrochemically “insulating”

protein shell and the direct electron transfer from the enzyme to the surface of GCE is usually quite difficult. Incorporation of  $\text{Mn}_2\text{O}_3$  nanofibers into this film ( $\text{Mn}_2\text{O}_3$ -GOD/GCE) results in a pair of well defined redox peaks with an anodic peak potential at -0.372 V and a cathodic peak potential at -0.433 V. Furthermore, at the  $\text{Mn}_2\text{O}_3$ -Ag nanofibers-GOD modified electrode ( $\text{Mn}_2\text{O}_3$ -Ag-GOD/GCE), an enhanced current signal and redox peaks can be observed with an anodic peak potential and a cathodic peak potential shifting to -0.394 V and -0.443 V, respectively. In addition, the redox peaks obtained at the  $\text{Mn}_2\text{O}_3$ -Ag-GOD/GCE are sharper and the peak currents are higher. The redox peaks may be assigned to the direct electrochemistry of GOD, which is the characteristic of reversible electron transfer process between the electroactive center, FAD, and the electrode. The reaction can be schematically expressed as follows:  $\text{GOD-FAD} + 2\text{H}^+ + 2\text{e}^- \longleftrightarrow \text{GOD-FADH}_2$  [87]. Thus, the  $\text{Mn}_2\text{O}_3$ -Ag nanofibers played an important role in facilitating the electron exchange between the GOD and electrode. As the direct electron transfer between GOD's redox center and the electrode can only happen when the distance between the redox center and the electrode is very small (less than 1.3 nm) and thus allows the electron transfer via a tunneling mechanism [88-90], the observed results in our study indicated that GOD and  $\text{Mn}_2\text{O}_3$ -Ag nanofibers are in close contact and thus  $\text{Mn}_2\text{O}_3$ -Ag nanofibers formed network provides numerous electron transfer pathways to "interconnect" the redox center within the enzyme and the surface of GCE. Such close contact between GOD and  $\text{Mn}_2\text{O}_3$ -Ag nanofibers could also favor the subsequent glucose detection through oxygen reduction because the glucose-oxidation (by GOD) induced local oxygen concentration change can be quickly monitored by  $\text{Mn}_2\text{O}_3$ -Ag nanofibers without signal loss due to the diffusion effect.

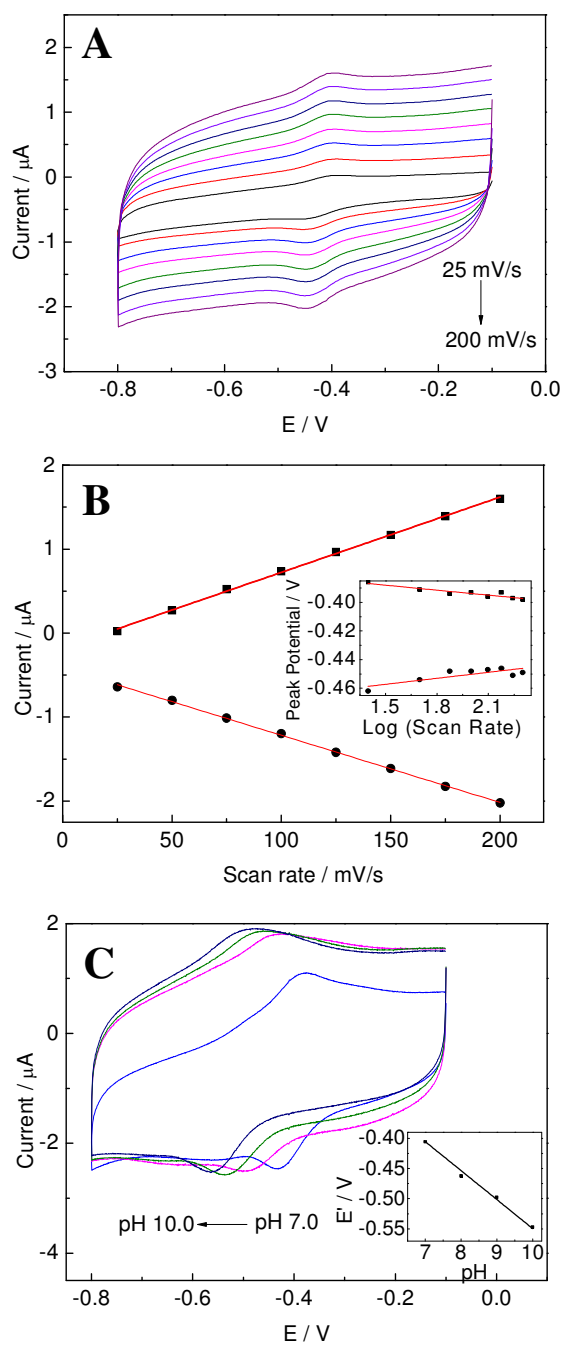


Figure 5. (A) CVs of the Mn<sub>2</sub>O<sub>3</sub>-Ag-GOD/GCE in N<sub>2</sub> de-aerated 0.1 M pH 7 phosphate buffer at the scan rates of 25, 50, 75, 100, 125, 150, 175 and 200 mV/s, respectively. (B) The plot of the peak current vs. scan rate; inset presents the relationship between the peak potential ( $E_p$ ) and the natural logarithm of scan rate. (C) CVs of the Mn<sub>2</sub>O<sub>3</sub>-Ag-GOD-/GCE in 0.1 M pH 7 phosphate buffer with pH values ranging from 7.0 to 10.0 (scan rates = 100 mV/s); inset presents the plot of the formal potential  $E^0$  vs. pH.

In order to determine the kinetic parameters of GOD at the Mn<sub>2</sub>O<sub>3</sub>-Ag-GOD/GCE, the effect of scan rate on the CV was investigated. The scan rates were investigated from 25 mV/s to 200 mV/s and the CVs were presented in Figure 5A. Both the reduction and oxidation peak currents increase linearly with the scan rate (Figure 5B), showing a typical surface controlled quasi-reversible electrochemical behavior. It further demonstrates the direct electrochemistry nature of GOD on the electrode. According to Faraday's law of electrolysis:  $Q = nFA\Gamma^*$ , where  $Q$  is the charge involved in the reaction,  $A$  is the electrode area,  $n$  is the number of electron transferred,  $F$  is the Faraday constant, and  $\Gamma^*$  is the surface coverage of the electroactive substance [91] and by integrating the reduction peak ( $7.06673 \times 10^{-7}$  C) in the CV, the surface coverage ( $\Gamma^*$ ) of electroactive GOD was estimated to be  $5.18 \times 10^{-11}$  mol/cm<sup>2</sup>, which is nearly 20-fold higher than  $2.86 \times 10^{-12}$  mol/cm<sup>2</sup> determined for GOD entrapped in Nafion on a bare GCE [92] [43]. The result indicates the effectiveness of the Mn<sub>2</sub>O<sub>3</sub>-Ag nanofibers with respect to mediating the electron transfer from GOD to the electrode.

Furthermore, as shown in the inset of Figure 5B, both the anodic and cathodic peak potentials show a linear relationship with the logarithm of scan rate, with slopes of  $-2.3RT/\alpha nF$  and  $2.3RT/(1-\alpha)nF$  for the cathodic peak and anodic peak, respectively, in which  $\alpha$  (the electron transfer coefficient) can be estimated to be 0.318. In order to calculate the electron transfer rate constant ( $k_s$ ), Laviron equation  $\log k_s = \alpha \log(1-\alpha) + (1-\alpha) \log \alpha - \log(2.3RT/nFv) - \alpha(1-\alpha)(nF\Delta E_p/2.3RT)$  was applied, where  $\alpha$  is the electron transfer coefficient,  $n$  is the electron transfer number,  $k_s$  is the electron transfer rate constant [93, 94],  $R$  is the gas constant,  $T$  is the thermodynamic temperature, and  $\Delta E_p$  is the peak-to-peak separation. The calculated  $k_s$  value ( $1.24 \text{ s}^{-1}$ ) for the Mn<sub>2</sub>O<sub>3</sub>-Ag-GOD

modified electrode is higher than or in the same range of other reported values in literature such as  $1.01 \text{ s}^{-1}$  for pCoTTP-SWNTs-GOD modified GCE,  $0.3 \text{ s}^{-1}$  for GOD at aligned SWNT arrays modified gold electrode,  $0.026 \text{ s}^{-1}$  for GOD-DTSSP modified gold electrode,  $1.56 \text{ s}^{-1}$  for boron doped CNT-GOD modified GCE,  $1.3 \text{ s}^{-1}$  for gold nanoparticles-GOD modified GCE,  $1.53 \pm 0.45 \text{ s}^{-1}$  CNTs- GOD modified GCE) [89, 95, 96], demonstrating that  $\text{Mn}_2\text{O}_3$ -Ag nanofibers provided a favorable microenvironment for enhancing the direct electron transfer, which is in good agreement with the results observed in Figure 4.

As the interconversion of the FAD/FADH<sub>2</sub> redox couple involves two electrons and two protons, the pH value of the solution could affect the electrochemical behavior of GOD. Figure 5C shows the pH-dependent GOD redox peak potential shift in the range from pH 7 to pH 10 (in de-aerated 0.1 M phosphate buffer solution). One can see that the increase of buffer pH caused a negative shift in redox peak potentials. For each pH value, formal potential ( $E^\circ$ ) of the redox couple is calculated and plotted against pH. As shown in the inset of Figure 5C, formal potential linearly changes with the pH value with a slope of  $-48 \text{ mV/pH}$  ( $R^2=0.999$ ). This slope is slightly smaller than the theoretical Nernstian value of  $-59.2 \text{ mV/pH}$  at room temperature ( $25 \text{ }^\circ\text{C}$ ) for a reversible two-electron, two-proton process. This might be attributed to the influence of the protonation of the water molecules coordinated with the surface of  $\text{Mn}_2\text{O}_3$  or Ag [97].

### ***2.2.3 Electrochemical reduction of $O_2$ at the modified electrodes and amperometric glucose biosensing***

To develop oxygen-reduction based glucose biosensor, the electrochemical reduction of oxygen on the  $Mn_2O_3$ -Ag-GOD modified electrodes towards oxygen reduction is shown in Figure 6A. As a comparison, the electrochemical reduction of oxygen on the  $Mn_2O_3$  nanofibers or  $Mn_2O_3$ -Ag nanofibers modified electrodes is presented in Figure 6. One can see that oxygen reduction on the  $Mn_2O_3$  nanofibers modified GCE starts at ca. -0.2 V, but no oxygen reduction peak is observed in the examined potential range (Figure 6A). In contrast,  $Mn_2O_3$ -Ag nanofibers modified GCE shows an obvious oxygen reduction peak centered at ca. -0.5 V (Figure 6B), accompanied by enhanced oxygen reduction current, which can be attributed to the incorporation of Ag in the  $Mn_2O_3$  nanofibers. Further incorporation of GOD into  $Mn_2O_3$ -Ag did not change the oxygen reduction performance except that a slightly decrease of oxygen reduction peak current

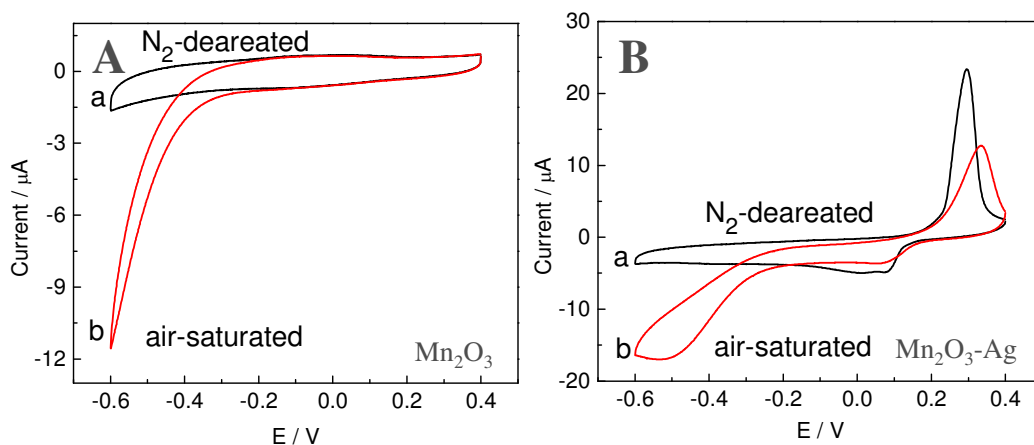


Figure 6. CVs of the (A)  $\text{Mn}_2\text{O}_3/\text{GCE}$  and (B)  $\text{Mn}_2\text{O}_3\text{-Ag}/\text{GCE}$  in  $\text{N}_2$  de-aerated (black) and air-saturated (red) 0.1 M pH 7 phosphate buffer solution at the scan rate of 100 mV/s.

was observed (Figure 7A), which may be ascribed to non-conductivity of the immobilized GOD. These results clearly demonstrate that on one hand,  $\text{Mn}_2\text{O}_3\text{-Ag}$  nanofibers possess a high electrocatalytical activity toward the oxygen reduction; on the other hand, they are an excellent biocompatible matrix for GOD immobilization as well as direct electron transfer. Such features could potentially enable enhanced glucose detection based on the reduction of oxygen because GOD-based glucose oxidation consumes oxygen.

The electrocatalytic properties of the modified electrodes towards glucose detection were further investigated by CVs. Figure 7B shows the CVs of the  $\text{Mn}_2\text{O}_3\text{-Ag-GOD}/\text{GCE}$  in the absence and presence of glucose in air-saturated phosphate buffer. With the addition of glucose, the dissolved oxygen is consumed for the oxidation of glucose by GOD. Thus the dissolved oxygen concentration decreases. Consequently, the peak current of oxygen reduction decreases [2]. This study also indicated that the immobilized

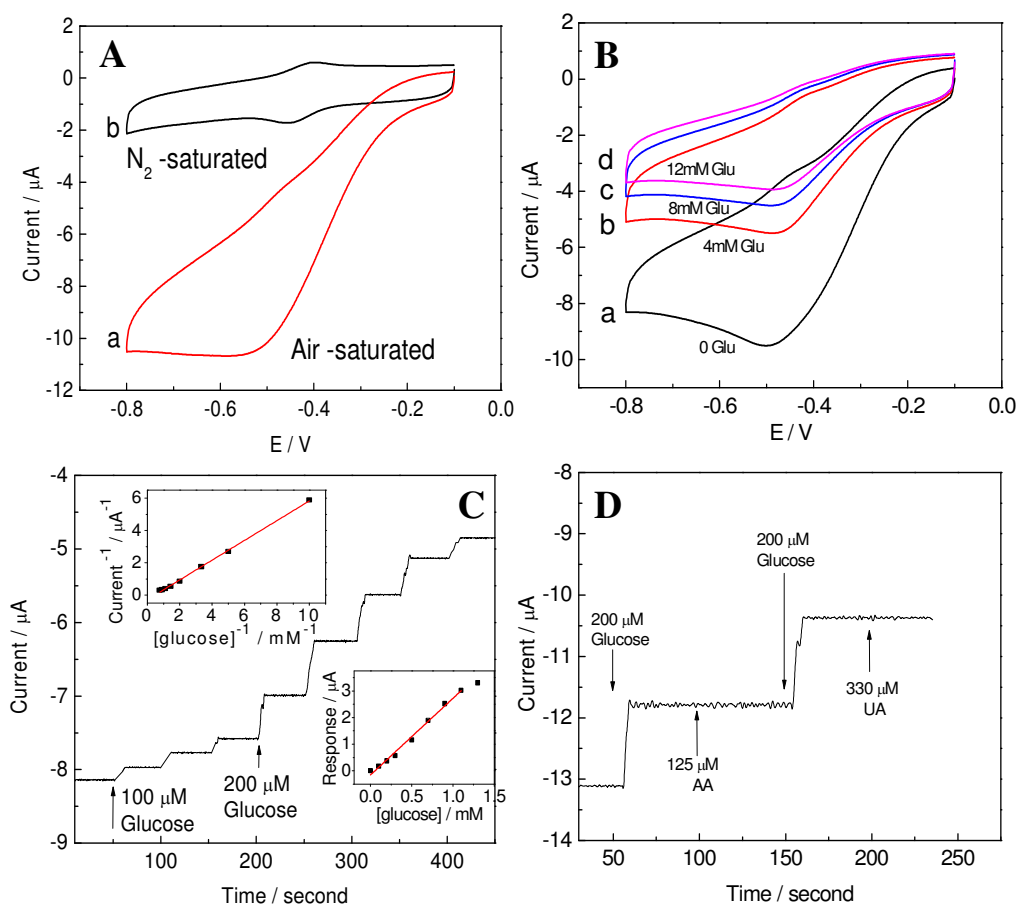


Figure 7. (A) CV curves at the  $\text{Mn}_2\text{O}_3\text{-Ag-GOD/GCE}$  in  $\text{N}_2$ -deaerated (black) and air-saturated (red) 0.1 M pH 7 phosphate buffer at the scan rate of 100 mV/s. (B) CV curves at the  $\text{Mn}_2\text{O}_3\text{-Ag-GOD/GCE}$  in air-saturated 0.1 M pH 7 phosphate buffer in the presence of 0 mM, 4 mM, 8 mM, and 12 mM glucose (scan rate = 100 mV/s). (C) Amperometric response to successive addition of 0.1 mM and 0.2 mM glucose on the  $\text{Mn}_2\text{O}_3\text{-Ag-GOD/GCE}$  at an applied potential of  $-0.45$  V vs. Ag/AgCl. Insets are the calibration plot for glucose (upper left corner) and the Lineweaver–Burk plot (lower right corner), respectively. (D) Amperometric response of the  $\text{Mn}_2\text{O}_3\text{-Ag-GOD/GCE}$  to 0.2 mM glucose, 0.125 mM AA, 0.2mM glucose and 0.33 mM UA, respectively.

GOD still maintains its activity. According to the CV results shown in Figure 7B, amperometric glucose detection was carried out in an air-saturated 0.1 M pH 7 phosphate buffer solution at an applied potential of  $-0.45$  V (vs. Ag/AgCl) under continuously stirring. This applied potential corresponds to the oxygen reduction peak potential for 4 mM glucose in Figure 7B. Figure 7C shows the amperometric responses of the  $\text{Mn}_2\text{O}_3\text{-}$

Ag-GOD/GCE to the successive addition of 0.1 mM and 0.2 mM glucose. It can be seen that the glucose biosensor responds rapidly to the injection of glucose, reaching steady-state current within 5-10 s (depending on the glucose concentration) after each injection. The fast response could be ascribed to a fast electron transfer and good electrocatalytic property provided by Mn<sub>2</sub>O<sub>3</sub>-Ag nanofibers and the close contact between GOD and Mn<sub>2</sub>O<sub>3</sub>-Ag nanofibers. The close contact between GOD and Mn<sub>2</sub>O<sub>3</sub>-Ag nanofibers allows the glucose oxidation-induced oxygen concentration change being quickly monitored, and the signal can be transferred to GCE through numerous electron transfer pathways provided by Mn<sub>2</sub>O<sub>3</sub>-Ag nanofibers network. The detection limit obtained on the Mn<sub>2</sub>O<sub>3</sub>-Ag nanofibers modified electrode at -0.45 V is 1.73 μM (S/N=3), which is among the best reported values for oxygen-reduction based GOD biosensors [98, 99]. The corresponding calibration curve is presented as the inset in the lower right corner of Figure 7C and shows a linear range up to 1.1 mM ( $R^2 = 0.99$ ) with a high sensitivity of 40.60 μA·mM<sup>-1</sup>·cm<sup>-2</sup>, which are highly competitive with other reported values in literature [31, 95, 96, 98]. The oxygen reduction-based glucose biosensors always show saturated response at relatively low glucose concentrations [87, 96, 100], resulting in much narrower linear range than other types of GOD-based glucose sensors (e.g. based on the detection of H<sub>2</sub>O<sub>2</sub> oxidation). Such phenomena can be explained by the low dissolved oxygen concentration in aqueous solution and fast oxygen consumption through enzymatic-based glucose oxidation. To calculate the apparent Michaelis–Menten constant ( $K_{m,app}$ ), the Lineweaver–Burk plot was applied and presented as the inset in the upper left corner of Figure 7C. The  $K_{m,app}$  value of the glucose sensor was determined to be 2.1 mM. This value is around the average value of the affinities recorded for some

recently reported GOD-based biosensor (e.g. 0.98 mM for pCoTTP/SWNTs/Nafion/GOD modified electrode [96]; 1.1 mM for cellulose/MWCNT/GOD modified electrode [101]; 2.4 mM for a MWCNT/Celestine blue/sol-gel/GOD modified electrodes[102]; and 5.1 mM for a CdS nanoparticles/GOD modified electrode [103]). Such low  $K_{m,app}$  value indicates a high affinity between the enzyme and substrate, which may be attributed to the good biocompatibility of the  $Mn_2O_3$ -Ag nanofibers. To the best of our efforts, various recently reported GOD glucose biosensors based on oxygen reduction are summarized in Table 2 with respect to the sensing material, sensing technique, the limit of detection (LOD), sensitivity, the linear range,  $K_{m,app}$ , and the electron transfer rate constant ( $k_s$ ). It can be seen that the performance of the developed glucose biosensor is among the best (Table 1) [96, 102-111].

The selectivity of the  $Mn_2O_3$ -Ag-GOD based glucose biosensor was also evaluated against UA and AA which are normally interfering species in the detection of glucose. As presented in Figure 6D, the as-developed glucose biosensor exhibits negligible response to the injection of UA and AA at their physiological concentration level. The excellent selectivity of the as-prepared glucose biosensor can be attributed to the low applied potential because UA and AA can not be oxidized at such low applied potential [57].

Table 2. Comparison of various GOD-based glucose biosensors based on oxygen reduction

Sensing materials	Sensing technique	LOD ( $\mu\text{M}$ )	Linear range	Sensitivity	$K_m^{\text{app}}$ (mM)	$K_s$ ( $\text{s}^{-1}$ )	Reference
Colloidal gold	Cyclic voltammetry	10	0.04 mM–0.28 mM	$8.4 \mu\text{A}\cdot\text{mM}^{-1}$	—	38.9	[115]
CdSnanoparticles	Cyclic voltammetry	50	0.5 mM–11.1 mM	$7 \mu\text{A}\cdot\text{mM}^{-1}$	5.1	—	[114]
CNTs	Amperometry (-0.48 V vs. Ag/ AgCl)	20	0.04 mM–1.0 mM	$2.4 \mu\text{A}\cdot\text{mM}^{-1}$	—	1.08	[116]
Colloidal gold/ DHP composite	Linear sweep voltammetry	100	0.5 mM–9.3 mM	$1.14 \mu\text{A}\cdot\text{mM}^{-1}$	—	1.713	[117]
Quantum dots/ CNTs	Cyclic voltammetry	—	up to 0.7 mM	$1.018 \mu\text{A}\cdot\text{mM}^{-1}$	0.651	—	[118]
Soluble carbon nanofibers	Amperometry (-0.3 V vs. SCE)	2.5	10 $\mu\text{M}$ –350 $\mu\text{M}$	$36.3 \mu\text{A}\cdot\text{cm}^{-2}\cdot\text{mM}^{-1}$	—	—	[119]
MWCNTs	Cyclic voltammetry	—	0.1 mM–5 mM	$16.25 \mu\text{A}\cdot\text{mM}^{-1}$	—	—	[120]
B-doped CNTs	Cyclic voltammetry	10	up to 0.3 mM	$111.57 \mu\text{A}\cdot\text{cm}^{-2}\cdot\text{mM}^{-1}$	—	1.56	[121]
pCoTTP/ SWCNTs	Amperometry (-0.2 V vs. Ag/ AgCl)	5.33	up to 1 mM	$16.57 \mu\text{A}\cdot\text{cm}^{-2}\cdot\text{mM}^{-1}$	0.98	1.01	[107]
Gelatin/ MWCNTs	Amperometry (-0.44 V vs. Ag/ AgCl)	10	6.3 mM–20.09 mM	$2.47 \mu\text{A}\cdot\text{cm}^{-2}\cdot\text{mM}^{-1}$	—	1.08	[122]
CNTs/ Celestine Blue	Amperometry (-0.35 V vs. Ag/ AgCl)	0.3	10 $\mu\text{M}$ –6 mM	$18.3 \mu\text{A}\cdot\text{mM}^{-1}$	2.4	1.26	[113]
$\text{Mn}_2\text{O}_3$ -Ag nanofibers	Amperometry (-0.45 V vs. Ag/ AgCl)	1.73	up to 1.1 mM	$40.6 \mu\text{A}\cdot\text{cm}^{-2}\cdot\text{mM}^{-1}$	2.1	1.24	this work

### **2.3 Conclusion**

Following a facile two-step procedure (electrospinning followed by calcination), novel functional  $\text{Mn}_2\text{O}_3$ -Ag nanofibers were fabricated. The electrochemical studies of the  $\text{Mn}_2\text{O}_3$ -Ag nanofibers-GOD modified electrode suggest that highly porous  $\text{Mn}_2\text{O}_3$ -Ag nanofibers could provide a favorable microenvironment for the GOD immobilization, stabilize its biological activity, and enhance the direct electron transfer of GOD to a large extent due to the high specific surface area, good biocompatibility and numerous efficient electron transfer pathways offered by  $\text{Mn}_2\text{O}_3$ -Ag nanofibers network. The observed enhanced direct electron transfer also indicated the close contact between GOD and  $\text{Mn}_2\text{O}_3$ -Ag nanofibers, which favors the glucose detection through oxygen reduction because the glucose-oxidation (by GOD) induced local oxygen concentration change can be quickly monitored on  $\text{Mn}_2\text{O}_3$ -Ag nanofibers without signal loss due to the diffusion. The as-prepared amperometric glucose biosensor based on  $\text{Mn}_2\text{O}_3$ -Ag nanofibers and GOD shows a fast response towards glucose injection with an excellent sensitivity and a good limit of detection. In addition, a low  $K_{m,app}$  value was also obtained for the developed system, indicating an excellent enzyme-substrate affinity. Furthermore, the glucose biosensor exhibits excellent selectivity as no interference from UA or AA was observed. All these features demonstrate that the  $\text{Mn}_2\text{O}_3$ -Ag nanofibers-GOD composite is a promising material for highly sensitive and selective electrochemical glucose detection based on oxygen reduction.

## *Chapter 3*

### *Conclusions, Future Prospects and Challenges*

In this work,  $\text{Mn}_2\text{O}_3$ -Ag nanofibers were fabricated by electrospinning PVP sol-gel solution containing  $\text{Mn}(\text{NO}_3)_2$  and  $\text{AgNO}_3$ , followed by calcination in air at  $500\text{ }^\circ\text{C}$  for 3 h. The as-prepared  $\text{Mn}_2\text{O}_3$ -Ag nanofibers were employed as the immobilization matrix for glucose oxidase (GOD) to construct an amperometric sensor for glucose detection in pH 7 phosphate buffer. The  $\text{Mn}_2\text{O}_3$ -Ag-GOD modified electrode demonstrated fast response to glucose, along with high sensitivity and excellent selectivity. Based on these good results, the  $\text{Mn}_2\text{O}_3$ -Ag nanofibers based composites were proved to be a promising biosensing platform for the construction of a GOD based glucose biosensor.

However, the GOD based biosensor for glucose detection suffers from several drawbacks that need to be addressed: (1) since oxidase-based biosensors rely on the use of oxygen as the physiological electron acceptor, they are subject to errors resulting from fluctuations in oxygen tension and/or the stoichiometric limitation of oxygen. (2) GOD can only maintain its catalytic activity in suitable pH, temperature and humidity. Such feature greatly limits the prevalent use of GOD based glucose sensor due to the low stability and reproducibility of GOD. In addition, toxic chemicals can impact the activity of GOD [1]. The first challenge can be potentially solved by several avenues: (1) The use of mass transport-limiting films (such as polyurethane or polycarbonate) for tailoring the flux of glucose and oxygen, i.e., increasing the oxygen/glucose permeability ratio. (2) It is also possible to circumvent the oxygen demand issue by replacing the GOD with glucose dehydrogenase (GDH), which does not require an oxygen cofactor. (3) Another

possible solution is to develop a reagentless glucose biosensor with a low operating potential, close to that of the redox potential of the enzyme. In this case, the electron could be transferred directly from glucose to the electrode via the active site of the enzyme. To address the second challenge, nonenzymatic glucose sensor may be a suitable solution as there is no biomolecule used in the biosensor fabrication, which could greatly improve the stability.

We strongly believe that, with the development of science and technology, significant advances are expected in a few years to improve current glucose detection technology and thus benefit hundred millions of diabetes patients.

## Reference

1. Wang, J., *Electrochemical Glucose Biosensors*. Chemical Reviews 2008; **108**: 814.
2. Li, F.H., J.X. Song, F. Li, X.D. Wang, Q.X. Zhang, D.X. Han, A. Ivaska, and L. Niu, *Direct Electrochemistry of Glucose Oxidase and Biosensing for Glucose Based on Carbon Nanotubes@SnO<sub>2</sub>-Au Composite*. Biosensors & Bioelectronics 2009; **25**: 883.
3. Cowie, C.C., K.F. Rust, D.D. Byrd-Holt, E.W. Gregg, E.S. Ford, L.S. Geiss, K.E. Bainbridge, and J.E. Fradkin, *Prevalence of Diabetes and High Risk for Diabetes Using A1c Criteria in the Us Population in 1988-2006*. Diabetes Care 2010; **33**: 562.
4. Newman, J.D. and A.P.F. Turner, *Home Blood Glucose Biosensors: A Commercial Perspective*. Biosensors & Bioelectronics 2005; **20**: 2435.
5. Wei, A., X.W. Sun, J.X. Wang, Y. Lei, X.P. Cai, C.M. Li, Z.L. Dong, and W. Huang, *Enzymatic Glucose Biosensor Based on ZnO Nanorod Array Grown by Hydrothermal Decomposition*. Applied Physics Letters 2006; **89**.
6. Wang, J.X., X.W. Sun, A. Wei, Y. Lei, X.P. Cai, C.M. Li, and Z.L. Dong, *Zinc Oxide Nanocomb Biosensor for Glucose Detection*. Applied Physics Letters 2006; **88**.
7. Ding, Y., Y. Wang, L. Su, M. Bellagamba, H. Zhang, and Y. Lei, *Electrospun Co<sub>3</sub>O<sub>4</sub> Nanofibers for Sensitive and Selective Glucose Detection*. Biosensors & Bioelectronics 2010; **Accepted**.
8. Wang, H.C., X.S. Wang, X.Q. Zhang, X. Qin, Z.X. Zhao, Z.Y. Miao, N. Huang, and Q. Chen, *A Novel Glucose Biosensor Based on the Immobilization of Glucose Oxidase onto Gold Nanoparticles-Modified Pb Nanowires*. Biosensors & Bioelectronics 2009; **25**: 142.
9. Deng, S.Y., G.Q. Jian, J.P. Lei, Z. Hu, and H.X. Ju, *A Glucose Biosensor Based on Direct Electrochemistry of Glucose Oxidase Immobilized on Nitrogen-Doped Carbon Nanotubes*. Biosensors & Bioelectronics 2009; **25**: 373.
10. Kong, T., Y. Chen, Y.P. Ye, K. Zhang, Z.X. Wang, and X.P. Wang, *An Amperometric Glucose Biosensor Based on the Immobilization of Glucose Oxidase on the ZnO Nanotubes*. Sensors and Actuators B-Chemical 2009; **138**: 344.
11. Heller, A. and B. Feldman, *Electrochemical Glucose Sensors and Their Applications in Diabetes Management*. Chemical Reviews 2008; **108**: 2482.
12. Bankar, S.B., M.V. Bule, R.S. Singhal, and L. Ananthanarayan, *Glucose Oxidase - an Overview*. Biotechnology Advances 2009; **27**: 489.
13. Wilson, R. and A.P.F. Turner, *Glucose Oxidase: An Ideal Enzyme*. Biosensors & Bioelectronics 1992; **7**: 165.
14. Yoo, E.H. and S.Y. Lee, *Glucose Biosensors: An Overview of Use in Clinical Practice*. Sensors 2010; **10**: 4558.

15. Gamburgzev, S., P. Atanasov, and E. Wilkins, *Glucose Biosensor Based on Oxygen-Electrode .3. Long-Term Performance of the Glucose Biosensor in Blood-Plasma at Body-Temperature*. Analytical Letters 1995; **28**: 1143.
16. Gamburgzev, S., P. Atanasov, and E. Wilkins, *Performance of Glucose Biosensor Based on Oxygen Electrode in Physiological Fluids and at Body Temperature*. Sensors and Actuators B-Chemical 1996; **30**: 179.
17. Gamburgzev, S., P. Atanasov, and E. Wilkins, *Oxygen Electrode with Pyrolyzed Cotmppp Catalyst: Application in Glucose Biosensor*. Analytical Letters 1997; **30**: 503.
18. Yang, S.P., C. Salehi, P. Atanasov, and E. Wilkins, *Glucose Biosensor Based on Oxygen Electrode .4. In Vivo Evaluation of the Rechargeable Glucose Sensor*. Analytical Letters 1996; **29**: 1081.
19. Du, P., B. Zhou, and C.X. Cai, *Development of an Amperometric Biosensor for Glucose Based on Electrocatalytic Reduction of Hydrogen Peroxide at the Single-Walled Carbon Nanotube/Nile Blue a Nanocomposite Modified Electrode*. Journal of Electroanalytical Chemistry 2008; **614**: 149.
20. Celej, M.S. and G. Rivas, *Amperometric Glucose Biosensor Based on Gold-Dispersed Carbon Paste*. Electroanalysis 1998; **10**: 771.
21. Cespedes, F., E. Martinezfabregas, and S. Alegret, *Amperometric Glucose Biosensor Based on an Electrocatalytically Bulk-Modified Epoxy-Graphite Biocomposite*. Analytica Chimica Acta 1993; **284**: 21.
22. Dai, Y.Q. and K.K. Shiu, *Highly Sensitive Amperometric Glucose Biosensor Based on Glassy Carbon Electrode with Copper/Palladium Coating*. Electroanalysis 2004; **16**: 1806.
23. Karyakin, A.A., O.V. Gitelmacher, and E.E. Karyakina, *A High-Sensitive Glucose Amperometric Biosensor Based on Prussian-Blue Modified Electrodes*. Analytical Letters 1994; **27**: 2861.
24. Liu, G.D. and Y.H. Lin, *Amperometric Glucose Biosensor Based on Self-Assembling Glucose Oxidase on Carbon Nanotubes*. Electrochemistry Communications 2006; **8**: 251.
25. Retama, J.R., E.L. Cabarcos, D. Mecerreyes, and B. Lopez-Ruiz, *Design of an Amperometric Biosensor Using Polypyrrole-Microgel Composites Containing Glucose Oxidase*. Biosensors & Bioelectronics 2004; **20**: 1111.
26. Rodriguez, M.C. and G.A. Rivas, *Amperometric Glucose Biosensor Based on the Deposition of Copper and Glucose Oxidase onto Glassy Carbon Transducer*. Analytical Letters 2000; **33**: 2373.
27. Turdean, G., I.C. Popescu, and L. Oniciu, *A Glucose Oxidase Co(Ii) Phthalocyanine Carbon Paste Biosensor for the Amperometric Detection of Glucose*. Revue Roumaine De Chimie 1998; **43**: 203.
28. Wang, Q.L., G.X. Lu, and B.J. Yang, *Hydrogen Peroxide Biosensor Based on Direct Electrochemistry of Hemoglobin Immobilized on Carbon Paste Electrode by a Silica Sol-Gel Film*. Sens. Actuator B: Chem. 2004; **99**: 50.
29. Zhang, C.X. and K. Wang, *An Amperometric Glucose Biosensor Incorporating a Permeable Pre-Oxidation Layer*. Analytical Letters 2002; **35**: 869.
30. Shen, J., L. Dudik, and C.C. Liu, *An Iridium Nanoparticles Dispersed Carbon Based Thick Film Electrochemical Biosensor and Its Application for a Single Use*,

- Disposable Glucose Biosensor*. Sensors and Actuators B-Chemical 2007; **125**: 106.
31. Park, J.Y., Y.H. Kim, A. Seong, and Y.J. Yoo, *Amperometric Determination of Glucose, Based on the Direct Electron Transfer between Glucose Oxidase and Tin Oxide*. Biotechnology and Bioprocess Engineering 2008; **13**: 431.
  32. Zhao, X.J., Z.B. Mai, X.H. Kang, and X.Y. Zou, *Direct Electrochemistry and Electrocatalysis of Horseradish Peroxidase Based on Clay-Chitosan-Gold Nanoparticle Nanocomposite*. Biosensors & Bioelectronics 2008; **23**: 1032.
  33. Shin, Y.J., M. Wang, and J. Kameoka, *Electrospun Nanofiber Biosensor for Measuring Glucose Concentration*. Journal of Photopolymer Science and Technology 2009; **22**: 235.
  34. Liu, Y., H. Teng, H.Q. Hou, and T.Y. You, *Nonenzymatic Glucose Sensor Based on Renewable Electrospun Ni Nanoparticle-Loaded Carbon Nanofiber Paste Electrode*. Biosensors & Bioelectronics 2009; **24**: 3329.
  35. Wang, W., L. Zhang, S. Tong, X. Li, and W. Song, *Three-Dimensional Network Films of Electrospun Copper Oxide Nanofibers for Glucose Determination*. Biosens. Bioelectron. 2009; **25**: 708.
  36. Crespilho, F.N., R.M. Iost, S.A. Travain, O.N. Oliveira, and V. Zucolotto, *Enzyme Immobilization on Ag Nanoparticles/Polyaniline Nanocomposites*. Biosensors & Bioelectronics 2009; **24**: 3073.
  37. Lu, X.B., J.H. Zhou, W. Lu, Q. Liu, and J.H. Li, *Carbon Nanofiber-Based Composites for the Construction of Mediator-Free Biosensors*. Biosensors & Bioelectronics 2008; **23**: 1236.
  38. Jin, W., U. Wollenberger, and F.W. Scheller, *Pqq as Redox Shuttle for Quinoprotein Glucose Dehydrogenase*. Biological Chemistry 1998; **379**: 1207.
  39. Zayats, M., E. Katz, R. Baron, and I. Willner, *Reconstitution of Apo-Glucose Dehydrogenase on Pyrroloquinoline Quinone-Functionalized Au Nanoparticles Yields an Electrically Contacted Biocatalyst*. Journal of the American Chemical Society 2005; **127**: 12400.
  40. Raitman, O.A., F. Patolsky, E. Katz, and I. Willner, *Electrical Contacting of Glucose Dehydrogenase by the Reconstitution of a Pyrroloquinoline Quinone-Functionalized Polyaniline Film Associated with an Au-Electrode: An in Situ Electrochemical Spr Study*. Chemical Communications 2002: 1936.
  41. Bartlett, P.N., E. Simon, and C.S. Toh, *Modified Electrodes for Nadh Oxidation and Dehydrogenase-Based Biosensors*. Bioelectrochemistry 2002; **56**: 117.
  42. Park, S., H. Boo, and T.D. Chung, *Electrochemical Non-Enzymatic Glucose Sensors*. Analytica Chimica Acta 2006; **556**: 46.
  43. VASSILYEV, Y.B., *Kinetics and Mechanism of Glucose Electrooxidation on Different Electrode-Catalysts .1. Adsorption and Oxidation on Platinum*. JOURNAL OF ELECTROANALYTICAL CHEMISTRY 1985; **196**: 105.
  44. VASSILYEV, Y.B., *Kinetics and Mechanism of Glucose Electrooxidation on Different Electrode-Catalysts .2. Effect of the Nature of the Electrode and the Electrooxidation Mechanism*. JOURNAL OF ELECTROANALYTICAL CHEMISTRY 1985; **196**: 127.

45. Li, Y., Y.Y. Song, C. Yang, and X.H. Xia, *Hydrogen Bubble Dynamic Template Synthesis of Porous Gold for Nonenzymatic Electrochemical Detection of Glucose*. *Electrochemistry Communications* 2007; **9**: 981.
46. Park, S., T.D. Chung, and H.C. Kim, *Nonenzymatic Glucose Detection Using Mesoporous Platinum*. *Analytical Chemistry* 2003; **75**: 3046.
47. You, T.Y., O. Niwa, Z.L. Chen, K. Hayashi, M. Tomita, and S. Hirono, *An Amperometric Detector Formed of Highly Dispersed Ni Nanoparticles Embedded in a Graphite-Like Carbon Film Electrode for Sugar Determination*. *Analytical Chemistry* 2003; **75**: 5191.
48. Nagy, L., G. Nagy, and P. Hajos, *Copper Electrode Based Amperometric Detector Cell for Sugar and Organic Acid Measurements*. *Sensors and Actuators B-Chemical* 2001; **76**: 494.
49. Sun, Y.P., H. Buck, and T.E. Mallouk, *Combinatorial Discovery of Alloy Electrocatalysts for Amperometric Glucose Sensors*. *Analytical Chemistry* 2001; **73**: 1599.
50. Yeo, I.H. and D.C. Johnson, *Electrochemical Response of Small Organic Molecules at Nickel-Copper Alloy Electrodes*. *Journal of Electroanalytical Chemistry* 2001; **495**: 110.
51. Tominaga, M., T. Shimazoe, M. Nagashima, H. Kusuda, A. Kubo, Y. Kuwahara, and I. Taniguchi, *Electrocatalytic Oxidation of Glucose at Gold-Silver Alloy, Silver and Gold Nanoparticles in an Alkaline Solution*. *Journal of Electroanalytical Chemistry* 2006; **590**: 37.
52. Park, S., H. Boo, and T.D. Chung, *Electrochemical Non-Enzymatic Glucose Sensors*. *Anal. Chim. Acta* 2006; **556**: 46.
53. Ye, J.S., Y. Wen, W.D. Zhang, L.M. Gan, G.Q. Xu, and F.S. Sheu, *Nonenzymatic Glucose Detection Using Multi-Walled Carbon Nanotube Electrodes*. *Electrochemistry Communications* 2004; **6**: 66.
54. Zhuang, Z.J., X.D. Su, H.Y. Yuan, Q. Sun, D. Xiao, and M.M.F. Choi, *An Improved Sensitivity Non-Enzymatic Glucose Sensor Based on a Cu Nanowire Modified Cu Electrode*. *Analyst* 2008; **133**: 126.
55. Wang, J.X., X.W. Sun, X.P. Cai, Y. Lei, L. Song, and S.S. Xie, *Nonenzymatic Glucose Sensor Using Freestanding Single-Wall Carbon Nanotube Films*. *Electrochemical and Solid State Letters* 2007; **10**: J58.
56. Ding, Y., Y. Wang, L. Su, H. Zhang, and Y. Lei, *Preparation and Characterization of Ni-Ag Nanofibers, Ni Nanofibers, and Porous Ag: Towards the Development of Highly Sensitive and Selective Non-Enzymatic Glucose Sensor*. *Journal of Materials Chemistry* 2010; **Submitted**.
57. Reitz, E., W.Z. Jia, M. Gentile, Y. Wang, and Y. Lei, *Cuo Nanospheres Based Nonenzymatic Glucose Sensor*. *Electroanalysis* 2008; **20**: 2482.
58. Wang, W., L. Zhang, S. Tong, X. Li, and W. Song, *Three-Dimensional Network Films of Electrospun Copper Oxide Nanofibers for Glucose Determination*. *Biosens Bioelectron* 2009; **25**: 708.
59. Chen, Q., J. Wang, G. Rayson, B. Tian, and Y. Lin, *Sensor Array for Carbohydrates and Amino Acids Based on Electrocatalytic Modified Electrodes*. *Analytical Chemistry* 1993; **65**: 251.

60. Zhu, H., X.Q. Lu, M.X. Li, Y.H. Shao, and Z.W. Zhu, *Nonenzymatic Glucose Voltammetric Sensor Based on Gold Nanoparticles/Carbon Nanotubes/Ionic Liquid Nanocomposite*. *Talanta* 2009; **79**: 1446.
61. Zhang, X.J., G.F. Wang, W. Zhang, Y. Wei, and B. Fang, *Fixure-Reduce Method for the Synthesis of Cu<sub>2</sub>O/Mwcnts Nanocomposites and Its Application as Enzyme-Free Glucose Sensor*. *Biosensors & Bioelectronics* 2009; **24**: 3395.
62. Chen, J., W.D. Zhang, and J.S. Ye, *Nonenzymatic Electrochemical Glucose Sensor Based on MnO<sub>2</sub>/Mwnts Nanocomposite*. *Electrochemistry Communications* 2008; **10**: 1268.
63. Shichiri, M., R. Kawamori, Y. Yamasaki, N. Hakui, and H. Abe, *Wearable Artificial Endocrine Pancreas with Needle-Type Glucose Sensor*. *Lancet* 1982; **2**: 1129.
64. Albisser, A.M., B.S. Leibel, T.G. Ewart, Z. Davidovac, C.K. Botz, W. Zingg, H. Schipper, and R. Grander, *Clinical Control of Diabetes by the Artificial Pancreas*. *Diabetes* 1974; **23**: 397.
65. Henry, C., *Getting under the Skin: Implantable Glucose Sensors*. *Analytical Chemistry* 1998; **70**: 594a.
66. Csoregi, E., D.W. Schmidtke, and A. Heller, *Design and Optimization of a Selective Subcutaneously Implantable Glucose Electrode Based on Wired Glucose-Oxidase*. *Analytical Chemistry* 1995; **67**: 1240.
67. Schmidtke, D.W., A.C. Freeland, A. Heller, and R.T. Bonnecaze, *Measurement and Modeling of the Transient Difference between Blood and Subcutaneous Glucose Concentrations in the Rat after Injection of Insulin*. *Proceedings of the National Academy of Sciences of the United States of America* 1998; **95**: 294.
68. Cox, M., *An Overview of Continuous Glucose Monitoring Systems*. *J. Pediatr. Health care* 2009; **23**: 344.
69. Hashiguchi, Y., T. Uemura, M. Sakakida, K. Kajiwara, K. Nishida, and M. Shichiri, *Development of a Miniaturized Glucose Monitoring-System by Combining a Needle-Type Glucose Sensor with Microdialysis Sampling Method - Long-Term Subcutaneous Tissue Glucose Monitoring in Ambulatory Diabetic-Patients*. *Diabetes Care* 1994; **17**: 387.
70. Poscia, A., M. Mascini, D. Moscone, M. Luzzana, G. Caramenti, P. Cremonesi, F. Valgimigli, C. Bongiovanni, and M. Varalli, *A Microdialysis Technique for Continuous Subcutaneous Glucose Monitoring in Diabetic Patients (Part 1)*. *Biosensors & Bioelectronics* 2003; **18**: 891.
71. Klonoff, D.C., *Noninvasive Blood Glucose Monitoring*. *Diabetes Care* 1997; **20**: 433.
72. Oliver, N.S., C. Toumazou, A.E.G. Cass, and D.G. Johnston, *Glucose Sensors: A Review of Current and Emerging Technology*. *Diabetic Medicine* 2009; **26**: 197.
73. Barnikol, W.K.R. and N. Weiler, *Experiments Aimed at Enabling the Development of an Implantable Glucose Sensor-Based on Polarimetry*. *Biomedizinische Technik* 1995; **40**: 114.
74. King, T.W., G.L. Cote, R. McNichols, and M.J. Goetz, *Multispectral Polarimetric Glucose Detection Using a Single Pockels Cell*. *Optical Engineering* 1994; **33**: 2746.

75. Goetz, M.J., G.L. Cote, R. Erckens, W. March, and M. Motamedi, *Application of a Multivariate Technique to Raman-Spectra for Quantification of Body Chemicals*. Ieee Transactions on Biomedical Engineering 1995; **42**: 728.
76. Gabriely, I., R. Wozniak, M. Mevorach, J. Kaplan, Y. Aharon, and H. Shamon, *Performance of a Novel near-Infrared (Nir) Transcutaneous Glucose (G) Monitor During Hypoglycemia*. Diabetes 1999; **48**: A99.
77. MacKenzie, H.A., H.S. Ashton, S. Spiers, Y.C. Shen, S.S. Freeborn, J. Hannigan, J. Lindberg, and P. Rae, *Advances in Photoacoustic Noninvasive Glucose Testing*. Clinical Chemistry 1999; **45**: 1587.
78. Larin, K.V., M.S. Eledrisi, M. Motamedi, and R.O. Esenaliev, *Noninvasive Blood Glucose Monitoring with Optical Coherence Tomography - a Pilot Study in Human Subjects*. Diabetes Care 2002; **25**: 2263.
79. Li, D. and Y.N. Xia, *Electrospinning of Nanofibers: Reinventing the Wheel?* Advanced Materials 2004; **16**: 1151.
80. Doshi, J. and D.H. Reneker, *Electrospinning Process and Applications of Electrospun Fibers*. Journal of Electrostatics 1995; **35**: 151.
81. Xie, J.W., X.R. Li, and Y.N. Xia, *Putting Electrospun Nanofibers to Work for Biomedical Research*. Macromolecular Rapid Communications 2008; **29**: 1775.
82. Subbiah, T., G.S. Bhat, R.W. Tock, S. Pararneswaran, and S.S. Ramkumar, *Electrospinning of Nanofibers*. Journal of Applied Polymer Science 2005; **96**: 557.
83. Huang, Z.M., Y.Z. Zhang, M. Kotaki, and S. Ramakrishna, *A Review on Polymer Nanofibers by Electrospinning and Their Applications in Nanocomposites*. Composites Science and Technology 2003; **63**: 2223.
84. Yarin, A.L., S. Koombhongse, and D.H. Reneker, *Bending Instability in Electrospinning of Nanofibers*. Journal of Applied Physics 2001; **89**: 3018.
85. Bognitzki, M., T. Frese, M. Steinhart, A. Greiner, J.H. Wendorff, A. Schaper, and M. Hellwig, *Preparation of Fibers with Nanoscaled Morphologies: Electrospinning of Polymer Blends*. Polymer Engineering and Science 2001; **41**: 982.
86. Megelski, S., J.S. Stephens, D.B. Chase, and J.F. Rabolt, *Micro- and Nanostructured Surface Morphology on Electrospun Polymer Fibers*. Macromolecules 2002; **35**: 8456.
87. Bao, S.J., C.M. Li, J.F. Zang, X.Q. Cui, Y. Qiao, and J. Guo, *New Nanostructured Tio2 for Direct Electrochemistry and Glucose Sensor Applications*. Advanced Functional Materials 2008; **18**: 591.
88. Hecht, H.J., D. Schomburg, H. Kalisz, and R.D. Schimd, *The 3d Structure of Glucose Oxidase from Aspergillus Niger. Implications for the Use of God as a Biosensor Enzyme*. Biosens. Bioelectron. 1993; **8**: 197.
89. Liu, J.Q., A. Chou, W. Rahmat, M.N. Paddon-Row, and J.J. Gooding, *Achieving Direct Electrical Connection to Glucose Oxidase Using Aligned Single Walled Carbon Nanotube Arrays*. Electroanalysis 2005; **17**: 38.
90. Liu, J.Q., M.N. Paddon-Row, and J.J. Gooding, *Heterogeneous Electron-Transfer Kinetics for Flavin Adenine Dinucleotide and Ferrocene through Alkanethiol Mixed Monolayers on Gold Electrodes*. Journal of Physical Chemistry B 2004; **108**: 8460.

91. Ding, Y., Y. Wang, B. Li, and Y. Lei, *Electrospun Hemoglobin Microbelts Based Biosensor for Sensitive Detection of Hydrogen Peroxide and Nitrite*. *Biosens. Bioelectron.* 2010; **25**: 2009.
92. Zhang, J., M. Feng, and H. Tachikawa, *Layer-by-Layer Fabrication and Direct Electrochemistry of Glucose Oxidase on Single Wall Carbon Nanotubes*. *Biosensors & Bioelectronics* 2007; **22**: 3036.
93. Laviron, E., *Adsorption, Autoinhibition and Autocatalysis in Polarography and in Linear Potential Sweep Voltammetry*. *Journal of Electroanalytical Chemistry and Interfacial Electrochemistry* 1974; **52**: 355.
94. Laviron, E., *General Expression of the Linear Potential Sweep Voltammogram in the Case of Diffusionless Electrochemical Systems*. *Journal of Electroanalytical Chemistry and Interfacial Electrochemistry* 1979; **101**: 19.
95. Zhao, S., K. Zhang, Y. Bai, W.W. Yang, and C.Q. Sun, *Glucose Oxidase/Colloidal Gold Nanoparticles Immobilized in Nafion Film on Glassy Carbon Electrode: Direct Electron Transfer and Electrocatalysis*. *Bioelectrochemistry* 2006; **69**: 158.
96. Chen, W., Y. Ding, J. Akhigbe, C. Bruckner, C.M. Li, and Y. Lei, *Enhanced Electrochemical Oxygen Reduction-Based Glucose Sensing Using Glucose Oxidase on Nanodendritic Poly[Meso-Tetrakis(2-Thienyl)Porphyrinato]Cobalt(II)-Swnts Composite Electrodes*. *Biosensors & Bioelectronics* 2010; **26**: 504.
97. Shan, D., S.X. Wang, H.G. Xue, and S. Cosnier, *Direct Electrochemistry and Electrocatalysis of Hemoglobin Entrapped in Composite Matrix Based on Chitosan and  $\text{CaCO}_3$  Nanoparticles*. *Electrochemistry Communications* 2007; **9**: 529.
98. Wei, A., X.W. Sun, J.X. Wang, Y. Lei, X.P. Cai, C.M. Li, Z.L. Dong, and W. Huang, *Enzymatic Glucose Biosensor Based on ZnO Nanorod Array Grown by Hydrothermal Decomposition*. *Applied Physics Letters* 2006; **89**: 123902.
99. Ren, G.L., X.H. Xu, Q. Liu, J. Cheng, X.Y. Yuan, L.L. Wu, and Y.Z. Wan, *Electrospun Poly(Vinyl Alcohol)/Glucose Oxidase Biocomposite Membranes for Biosensor Applications*. *Reactive & Functional Polymers* 2006; **66**: 1559.
100. Salimi, A., R. Hallaj, S. Soltanian, and H. Mamkhezri, *Nanomolar Detection of Hydrogen Peroxide on Glassy Carbon Electrode Modified with Electrodeposited Cobalt Oxide Nanoparticles*. *Analytica Chimica Acta* 2007; **594**: 24.
101. Wu, X.E., F. Zhao, J.R. Varcoe, A.E. Thumser, C. Avignone-Rossa, and R.C.T. Slade, *Direct Electron Transfer of Glucose Oxidase Immobilized in an Ionic Liquid Reconstituted Cellulose-Carbon Nanotube Matrix*. *Bioelectrochemistry* 2009; **77**: 64.
102. Noorbakhsh, A., A. Salimi, and E. Sharifi, *Fabrication of Glucose Biosensor Based on Encapsulation of Glucose-Oxidase on Sol-Gel Composite at the Surface of Glassy Carbon Electrode Modified with Carbon Nanotubes and Celestine Blue*. *Electroanalysis* 2008; **20**: 1788.
103. Huang, Y.X., W.J. Zhang, H. Xiao, and G.X. Li, *An Electrochemical Investigation of Glucose Oxidase at a  $\text{Cu}$  Nanoparticles Modified Electrode*. *Biosensors & Bioelectronics* 2005; **21**: 817.

104. Liu, S.Q. and H.X. Ju, *Reagentless Glucose Biosensor Based on Direct Electron Transfer of Glucose Oxidase Immobilized on Colloidal Gold Modified Carbon Paste Electrode*. *Biosensors & Bioelectronics* 2003; **19**: 177.
105. Luo, X.L., A.J. Killard, and M.R. Smyth, *Reagentless Glucose Biosensor Based on the Direct Electrochemistry of Glucose Oxidase on Carbon Nanotube-Modified Electrodes*. *Electroanalysis* 2006; **18**: 1131.
106. Wu, Y.H. and S.S. Hu, *Direct Electrochemistry of Glucose Oxidase in a Colloid Au-Dihexadecylphosphate Composite Film and Its Application to Develop a Glucose Biosensor*. *Bioelectrochemistry* 2007; **70**: 335.
107. Liu, Q., X.B. Lu, J. Li, X. Yao, and J.H. Li, *Direct Electrochemistry of Glucose Oxidase and Electrochemical Biosensing of Glucose on Quantum Dots/Carbon Nanotubes Electrodes*. *Biosensors & Bioelectronics* 2007; **22**: 3203.
108. Wu, L., X.J. Zhang, and H.X. Ju, *Amperometric Glucose Sensor Based on Catalytic Reduction of Dissolved Oxygen at Soluble Carbon Nanofiber*. *Biosensors & Bioelectronics* 2007; **23**: 479.
109. Salimi, A., A. Noorbakhsh, H. Mamkhezri, and R. Ghavami, *Electrocatalytic Reduction of H<sub>2</sub>O<sub>2</sub> and Oxygen on the Surface of Thionin Incorporated onto Mwcnts Modified Glassy Carbon Electrode: Application to Glucose Detection*. *Electroanalysis* 2007; **19**: 1100.
110. Deng, C.Y., J.H. Chen, X.L. Chen, C.H. Mao, L.H. Nie, and S.Z. Yao, *Direct Electrochemistry of Glucose Oxidase and Biosensing for Glucose Based on Boron-Doped Carbon Nanotubes Modified Electrode*. *Biosensors & Bioelectronics* 2008; **23**: 1272.
111. Periasamy, A.P., Y.J. Chang, and S.M. Chen, *Amperometric Glucose Sensor Based on Glucose Oxidase Immobilized on Gelatin-Multiwalled Carbon Nanotube Modified Glassy Carbon Electrode*. *Bioelectrochemistry* 2011; **80**: 114.